Active Sites Engineering through Palladium-Phosphorus Synergy for Heterogeneously-Catalyzed Alkoxycarbonylation Reactions

*Arjun Neyyathala[1], Felix Jung[1], Claus Feldmann[1], Stephan A. Schunk[2,3,4], Schirin Hanf[1]**

[1]*Institute for Inorganic Chemistry, Karlsruhe Institute of Technology, Engesserstr. 15, 76131 Karlsruhe, Germany.*

[2]*BASF SE, Carl-Bosch Str. 38, 67056 Ludwigshafen, Germany.*

[3]*hte GmbH, the high throughput experimentation company, Kurpfalzring 104, 69123 Heidelberg, Germany.*

[4]*Institute of Chemical Technology, Faculty of Chemistry and Mineralogy, Leipzig University, Linnéstr. 3, 04103 Leipzig, Germany.*

KEYWORDS: Alkoxycarbonylation, heterogeneous catalysis, palladium phosphide, supported nanoparticles, element synergy.

ABSTRACT

Crystalline palladium phosphide (Pd_3P) nanoparticles on silica were investigated for the alkoxycarbonylation of aryl halides, providing a strategic approach for designing high-performance carbonylation catalysts. The synthesized Pd_3P/SiO_2 (5 wt.%) catalyst was characterized via PXRD, HAADF-STEM, HRTEM, EDX, CO chemisorption and ICP-AES analysis. The incorporation of phosphorus into the palladium matrix, which results in the formation of a Pd_3P phase, enhanced the intrinsic catalytic activity in the alkoxycarbonylation of aryl halides by more than two-fold compared to a traditional purely Pd-based heterogeneous catalyst. Moreover, Pd_3P/SiO_2 (5 wt.%) outperformed many reported heterogeneous catalysts as well as some commonly used homogeneous catalysts. The exceptional performance of palladium phosphide nanoparticles can be attributed to highly active and uniformly distributed Pd sites separated by phosphorus. This work highlights the potential of element synergy in developing highly efficient carbonylation catalysts by exploring Pd-P system in the alkoxycarbonylation reaction.

1. Introduction

Carbonylation reactions, which involve the addition of carbon monoxide to activated C–X (X = halide) bonds in the presence of a nucleophile (NuH), provide access to a diverse range of aliphatic and aromatic carboxylic acid derivatives, amides, and azides, and are therefore a very important class of industrially relevant transformations.[1–4] The products synthesized from carbonylation reactions can either be used directly or further processed for the production of pharmaceuticals, detergents, flavors, fragrances, polymers, etc.[2,3,5] In this context, molecular palladium catalysts, either pre-synthesized, such as [$PdCl_2$(dppp)] (dppp = 1,3-bis(diphenylphosphino)propane),[6] [$PdCl_2$(dcpp)] (dcpp = 1,3-bis(dicyclohexylphosphino)propane),[6] [$PdBrPh(PPh_3)_2$],[7] [$Pd(PPh_3)_4$],[8] [$PdCl_2(PCy_3)_2$],[9] [$Pd(2\text{-}(CH_3NH)Py\text{-}PPh_2)_2](OAc)_2$,[10] or formed *in-situ* during the reaction from palladium-based compounds, e.g. palladium acetate or chloride, in the presence of ligands, such as triphenylphosphine (PPh_3),[11] 1,1′-bis(diphenylphosphino)ferrocene (dppf),[12] 1,3-bis(dicyclohexylphosphino)propane,[13] 1,3-bis(diisobutylphosphino)propane (DIBPP),[14] 2,2′-bis(diphenylphosphino)-1,1′-binaphthyl (BINAP),[15] (9,9-dimethyl-9H-xanthene-4,5-diyl)bis(diphenylphosphane) (Xantphos),[16] etc. are known to exhibit excellent activities in carbonylation reactions.[17] Even though such homogeneous catalysts exhibit high activity and selectivity, they pose significant challenges in terms of catalyst handling, separation, and reuse. This ultimately leads to a loss of noble metal, product contamination, and, as a consequence, increased process costs.[1] One strategy to overcome these challenges is the development and use of high-performing heterogeneous catalysts, through which a facile handling, product separation, and catalyst reuse is possible.

Despite the well-established industrial significance of alkoxycarbonylation reactions, research on palladium-based heterogeneous catalysis remains significantly less explored compared to its

homogeneous counterparts. This can partly be attributed to the aggregation of Pd in the presence of CO in solid catalysts, which leads to the formation of catalytically inactive species and thereby limiting large-scale applications.[1,18] The alkoxycarbonylation of aryl chlorides using Pd supported on activated carbon (Pd/C), as reported by Dufaud *et al*., is one of the earliest studies in the field of heterogeneously catalyzed carbonylation reactions.[18] This work essentially paved the way for the development of Pd-based heterogeneous catalysts for alkoxycarbonylation reactions of aryl or alkyl halides. Based on these initial findings, in the past two decades many research groups have reported various heterogeneous/heterogenized alkoxycarbonylation catalysts. Some examples are supported palladium particles, such as Pd/C,[19] Pd/CeO_2,[20] Pd/ Fe_3O_4,[21] palladium supported on N-doped carbon (Pd/PdO@NGr-C),[22] porous organic cage-stabilized Pd nanoparticles (Pd@CC3-R–MeOH),[23] immobilized Pd complexes[24],[25] and Pd catalysts in the presence of ionic liquids.[4],[26] Although these examples highlight the research focus on developing heterogeneous alkoxycarbonylation reactions, most catalysts suffer from low activity or involve complex synthesis procedures. Furthermore, previous studies rarely investigated the intrinsic activity of catalysts or their reaction kinetics. This underscores the significant potential for developing highly active solid-state catalysts through assessible synthesis techniques and for conducting in-depth investigations into performance-related parameters in carbonylation chemistry.

A very effective approach for the development of highly active and selective heterogeneous catalysts is the strategic combination of a catalytically active metal with a p-block element, which enables the modulation of the metal centers' electronic and geometric properties.[27,28] Through this so called “d-block-p-block element combination strategy”, highly active ensembles or sites can be formed on the catalyst surface, thereby tuning the adsorption properties of substrates and

intermediates, which can ultimately lead to an enhancement of both catalytic activity and selectivity.[29,30] In this context, the incorporation of phosphorus or sulfur into metal matrices to form metal phosphides or sulfides has demonstrated exceptional catalytic performance and has been investigated across various catalytic reactions.[30–34] Notable examples highlighting the impact of surface motifs, engineered through phosphorus or sulfur incorporation, include the exceptional performance of spatially isolated metal trimers in bulk nickel phosphide catalysts (Ni_2P, Ni_5P_4)[35] and palladium sulfides supported on carbon nitrite (Pd_4S/C_3N_4 and Pd_3S/C_3N_4) [29] for the semi-hydrogenation of alkynes. Additionally the enhanced hydroformylation activity driven by Rh_4 tetrameric motifs in supported rhodium sulfides ($Rh_{17}S_{15}/SiO_2$),[30] and the selective tuning of electrocatalytic nitrate reduction reactions enabled by active nickel ensembles in nickel phosphide deposited on carbon (Ni_2P/C)[36] further highlight the significance of these structural modifications. However, not only do the spatial arrangements of the metal centers and the formation of unsaturated metal sites play a key role, but the underlying charge transfer processes between the metal and the p-block element are equally critical. These processes mimic the electronic metal-ligand interactions observed in classical molecular catalysts.[28,37] As a result, the combination of a metal with a p-block element can create a powerful synergy, which offers a significant potential for the development of high-performance heterogenous catalysts.[28,37]

Despite exhibiting excellent catalytic performances, metal phosphides have not, to the best of our knowledge, been reported in the context of alkoxycarbonylation reactions. Therefore, in this study, supported palladium phosphide (Pd_3P) nanoparticles were synthesized and successfully applied in the alkoxycarbonylation of aryl iodides, demonstrating superior activity compared to pure Pd nanoparticles and several reported heterogeneous and homogeneous catalysts. This investigation

provides valuable insights into the design of heterogeneous catalysts through the application of the d-block–p-block element combination strategy in carbonylation chemistry.

2. Experimental section

2.1. Materials

Palladium acetate ($Pd(OAc)_2$) with a purity ≥ 99.99 % and 85 wt.% phosphoric acid (H_3PO_4) were purchased from Sigma Aldrich and hydrochloric acid (37 %) from Thermo Scientific Chemicals. The support material silica (Cariact, Q 20 C) was purchased from Fuji Silysia Chemical Ltd. Triethylamine (purity 99 %) as well as *n*-decane were purchased from abcr and iodobenzene with a purity ≥ 99 % from TCI. Ethanol with a purity ≥ 99.8 % was obtained from Carl Roth and acetone (HPLC grade), which was used for the GC sample preparation, was purchased from Fischer Scientific GmbH. All chemicals were used without any further purification. The gases used for this work, hydrogen (purity 99.999 %) and carbon monoxide (purity 98 %) were purchased from Air Liquide.

2.2. Instruments and methods

2.2.1. Catalysts synthesis

The supported palladium phosphide catalyst was synthesized using a previously reported procedure.[38] In a typical synthesis of Pd_3P/SiO_2 (5 wt.% Pd), 100 mg $Pd(OAc)_2$ and 10 µL H_3PO_4 were dissolved in concentrated hydrochloric acid *via* sonication. This solution was then added drop wise to 0.94 g silica (incipient wetness impregnation) and dried at 60 °C for 12 h. The dried impregnated material was further thermally treated in pure hydrogen at 400 °C for 8 h, with a heating ramp of 50 °C/min. The thermal treatment of the dried impregnated precursors was carried

out in a quartz Schlenk tube, which was equipped with a pressure relief valve, after evacuation and under Ar atmosphere. Further, hydrogen gas was introduced and the flask was heated to the required temperature using a box furnace. To prevent any surface oxidation, the synthesized catalysts were stored in a glove box (MBraun) under argon atmosphere.

Supported palladium nanoparticles (Pd/SiO_2, 5 wt.% Pd) were synthesized in a similar manner, however without the addition of phosphoric acid.

2.2.2. Instruments

PXRD measurements were performed on a Stoe STADI-MP diffractometer operating with a Ge-monochromatized Cu source (λ=1.54178 Å) in transmission mode with measurements performed until a diffraction angle of $2\Theta = 90°$. TEM, STEM and EDXS analysis were performed with a FEI Osiris ChemiSTEM operated at an acceleration voltage of 200 kV. TEM images were obtained and analyzed using a Gatan BM Ultrascan CCD camera and Gatan Digital Micrograph 2.3. HAADF-STEM images were acquired using FEI TEM Imaging and Analysis 4.6. In order to determine the particle size distributions of the samples, measurement of 200 nanoparticle diameters per sample was carried out. Elemental mapping with EDXS was performed using a Bruker Super-X EDXS system and quantification of the data was performed in Bruker Esprit 2.3 using the Cliff-Lorimer method with theoretical k factors. In order to prepare the samples for the electron microscopy analysis, the catalysts were dispersed in ethanol and a drop was carefully added to a grid (Cu grids covered by amorphous carbon film) and subsequently dried at 60 °C overnight. The quantification of Pd in the samples was done via ICP-AES analysis performed using an iCap 6500 device from ThermoFisher Scientific. The samples for the analysis were dissolved in nitric acid, hydrofluoric acid and hydrochloric acid at 130 °C for 12 h using a digestion

system. CO chemisorption measurements were performed with an instrument made in house with an analyzer from Rosemount Xstream. The carbonylation products obtained from the catalytic tests were analyzed qualitatively and quantitatively using an Agilent GC MS model 8860 GC and 5977B MSD. In order to perform a quantitative analysis, *n*-decane was used as an internal standard. For a typical analysis, the product obtained from the catalyst testing was filtered using a syringe filter (0.2 µm) and 80 µL samples were added to 1mL of acetone in a GC vial. The GC MS device was equipped with a silica capillary column (ID: 0.25 mm, film thickness: 0.25 µm, and length: 30 m). An injection volume of 1 µL, split ratio of 1:100 and inlet temperature of 310 °C was used for the analysis.

2.2.3. Catalysts testing

Catalytic tests were performed in a Parr 5500 series compact reactor with 25 mL capacity equipped with an overhead stirrer. In a typical reaction, iodobenzene (1 mmol), tryethylamine (3 mmol), *n*-decane (100 µL) and the catalyst (0.5 mol % Pd) were added to ethanol (4 mL) in the reactor. Further the reactor was flushed 3 times with carbon monoxide and pressurized to the required pressure and heated to the reaction temperature. A stirring speed of 1000 rpm was used for all tests to ensure the desired dissolution of CO in the liquid reaction medium. After the reaction time, the heater was turned off and the reactor was allowed to cool down to ambient conditions. Prior to the opening of the reactor, the remaining gas was slowly released and the product obtained was filtered and analyzed *via* GC MS analysis.

The tests for the determination of the apparent activation energyies were performed with iodobenzene conversions lower than 30 %. In order to determine the turnover frequency of the Pd_3P/SiO_2 (5 wt.% Pd) and Pd/SiO_2 (5 wt.% Pd) catalysts, the dispersion values obtained from the

CO chemisorption measurements were used and the estimations were done at conversions lower than 30 %.

For the recovery and recycling tests of the catalysts, the catalysts were removed after the reaction from the liquid products through centrifugation at 12000 rpm, followed by washing with acetone for 3 times. The washed catalysts were dried at 60°C overnight and used for the next runs without any further activation steps.

3. Results and discussions

3.1. Catalyst preparation and characterization

Silica supported palladium phosphide nanoparticles with 5 wt. % Pd metal loading, Pd_3P/SiO_2 (5 wt.% Pd) were synthesized following a reported procedure.[38] Therefore, palladium acetate ($Pd(OAc)_2$) and phosphoric acid (H_3PO_4) with a Pd to P molar ratio of 3 were dissolved in hydrochloric acid (HCl) and impregnated on silica as support material. After drying, the impregnated support had undergone thermal treatment in pure hydrogen at 400 °C. The powder X-ray diffraction (PXRD) analysis of the sample confirmed the formation of phase pure Pd_3P on silica (Figure 1a), and the occurrence of very broad reflexes in the diffractogram indicates the formation of small crystallites of palladium phosphide. Similarly, the PXRD analysis of the reference catalyst, Pd/SiO_2 (5 wt.% Pd) was performed, whereby clear reflexes corresponding to the face-centered cubic structure of palladium were observed (Figure S1). High resolution transmission electron microscope (HRTEM) analysis performed for Pd_3P/SiO_2 (5 wt.% Pd) indicated a lattice fringe distance of 2.0 Å, which aligns with the d spacing of Pd_3P (122) (Figure 1b). This finding, in addition to the PXRD analysis, provides conclusive proof for the formation of targeted Pd_3P phase. Further, energy dispersive X-ray analysis (EDX) in connection with TEM

imaging showed a uniform distribution of phosphorus and palladium on silica (Figure 2), with an average Pd/P ratio of 3.03, which is again in line with the elemental ratio of the targeted phase.

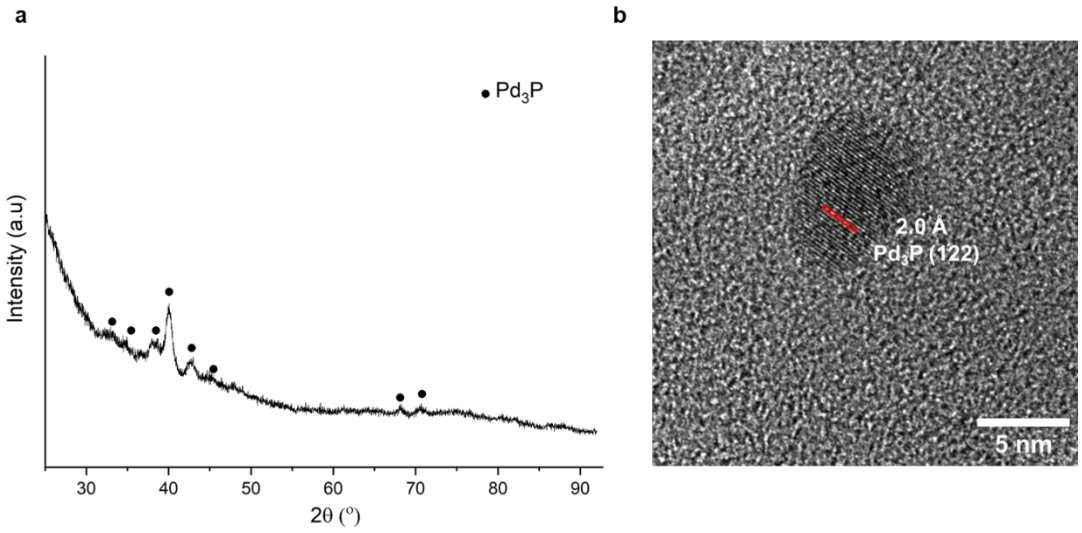

Figure 1: Phase identification of Pd_3P/SiO_2 (5 wt.% Pd) through a) powder X-ray diffraction and b) HRTEM lattice fringe-based assessment. (Pd_3P: ICSD 85525)

Spherical shaped particles with an average particle size of 5.56 nm uniformly distributed over the silica support were observed through high angle annular dark field scanning transmission electron microscopy (HAADF-STEM) imaging of Pd_3P/SiO_2 (5 wt.% Pd), whereas slightly bigger particles with an average size of 6.58 nm were identified for the pure palladium-based catalyst, Pd/SiO_2 (5 wt.% Pd). The difference in particle size of palladium phosphide and palladium nanoparticle can be attributed to the reduced crystallization ability of the Pd_3P phase,[39] which results in the formation of smaller crystallites even at a temperature of 400 °C, where the thermal treatment was carried out and the phase formation took place. For the determination of the metal dispersion of the catalysts, CO chemisorption measurements were performed. Surprisingly, a slightly reduced dispersion of 8.5 % was observed for Pd_3P/SiO_2 (5 wt.% Pd) in comparison to 9.5 % for Pd/SiO_2 (5 wt.% Pd), even though comparatively smaller nanoparticles were observed via HAADF-STEM

for the palladium phosphide catalyst (Table S1). This could be due to remaining P-species on the surface of Pd_3P due to the thermal treatment being carried out under stagnant condition. Since the catalytic reaction is carried out in solution, a surface cleaning can occur under reaction conditions.

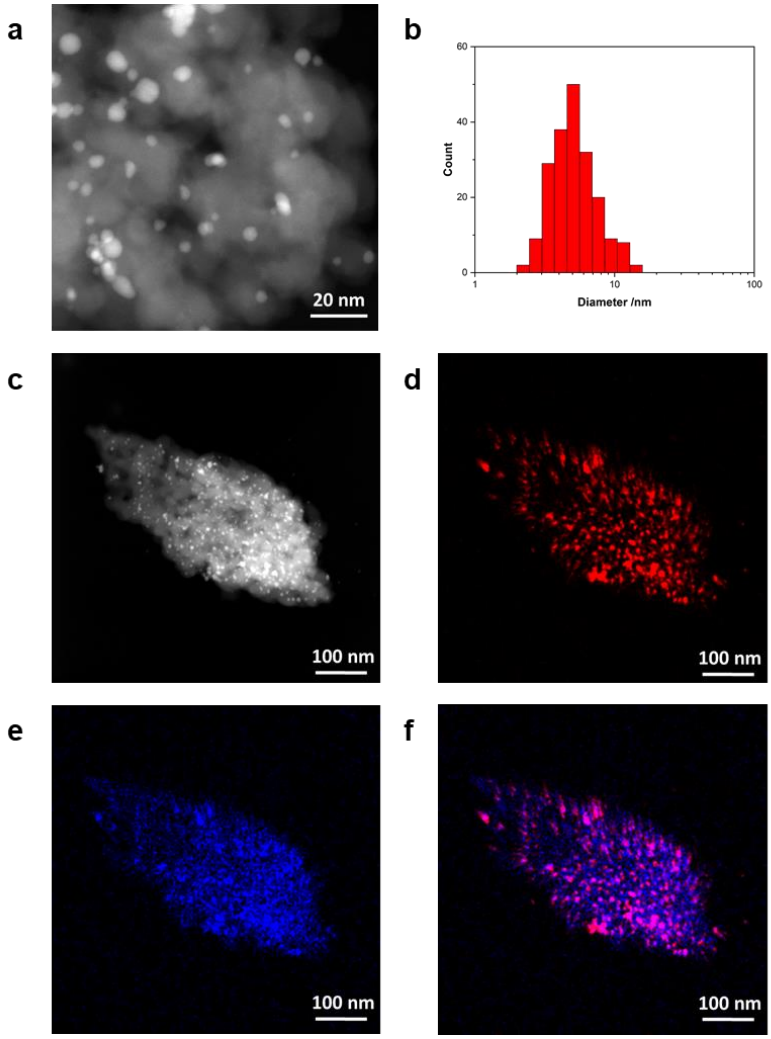

Figure 2: Transmission electron microscopy imaging of Pd_3P/SiO_2 (5 wt.% Pd) with a) HAADF-STEM images showing the distribution of spherical palladium phosphide nanoparticles on silica, b) the particle size distribution histogram, c) a HAADF-STEM image for the EDX mapping of d) palladium, e) phosphorus, and f) combined Pd and P (Pd: red, P: blue).

To quantify the Pd loading on silica for the Pd_3P/SiO_2 (5 wt.% Pd) catalyst, inductively coupled plasma–atomic emission spectroscopy (ICP–AES) analysis was performed. The Pd loading on silica was determined as 4.95 wt. %.

3.2. Alkoxycarbonylation reactions

The synthesized supported palladium phosphide catalyst, Pd_3P/SiO_2 (5 wt.% Pd) was applied in the alkoxycarbonylation reaction of iodobenzene. Initial experiments were performed at 100 °C with CO pressure of 6 bar, 3 equivalents (in comparison to iodobenzene) of triethylamine (Et_3N) as base, and ethanol as the solvent and nucleophile (NuH) in batch mode. Under these applied reaction conditions, an excellent iodobenzene conversion of 97 % with 100 % selectivity to ethyl benzoate (Table 1, entry 1) was observed. A complete conversion was achieved on extending the reaction time to 3 h (Table 1, entry 2). This provides an initial indication that the active catalyst synthesis strategy, based on the d-block and p-block element combinations, which has been successfully applied in hydroformylation,[30,31] hydrogenation,[29] and electrocatalysis,[36] can also be effectively translated to alkoxycarbonylation chemistry.

To investigate the necessity of the base in the alkoxycarbonylation reaction, a test was performed with the above mentioned reaction condition but without the addition of the base. A significantly reduced iodobenzene conversion of only 7% to ethyl benzoate was observed after 2 hours reaction time (Table 1, entry 3), pointing towards the importance of the base in the reaction. We attribute the necessity of a base in this reaction to the reaction mechanism of the alkoxycarbonylation of aryl halides (Figure S6). The base facilitates the decomposition of the acyl-palladium complex ($ArCO(L_n)PdX$) by promoting ester formation through the alcohol, while simultaneously neutralizing the generated HX. This process is crucial for regenerating the active Pd(0) species,

which can then enter the next catalytic cycle.[1,3,9,40,41] Moreover, the addition of a base can also significantly influence the rate determining step and the rate of the reaction itself.[42] This highlights the necessity of incorporating a base into the reaction system to complete the catalytic cycle, enhance the reaction rate, and achieve higher conversion levels. To investigate this fact further, various bases, including NaOAc, KOH, and K_2CO_3, were screened to evaluate their impact on the catalytic activity and identify the most suitable base for further studies. By performing the reaction with Et_3N a 97 % conversion of iodobenzene could be achieved, whereas NaOAc, KOH, and K_2CO_3 only resulted in lower conversions of 40 %, 70 % and 56 %, respectively (Table 1, entries 4, 5, and 6), possibly due to the superior solubility of tryethylamine in the reaction medium in comparison to the other bases. Similar trends, where Et_3N outperforms other bases, have been reported in previous studies on heterogeneously catalyzed alkoxycarbonylation reactions.[43,44] Hence all subsequent catalytic reactions were performed with Et_3N as the base.

Table 1: Alkoxycarbonylation reaction of iodobenzene with various bases and catalysts performed in batch mode.

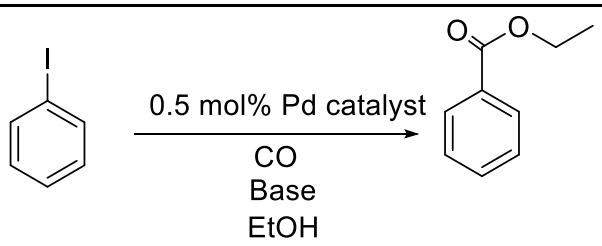

Entry	Catalyst	Base	Reaction time (h)	Iodobenzene conversion (%)
1	Pd_3P/SiO_2 (5 wt.% Pd)	Et_3N	2	97
2	Pd_3P/SiO_2 (5 wt.% Pd)	Et_3N	3	100
3	Pd_3P/SiO_2 (5 wt.% Pd)	-	3	7
4	Pd_3P/SiO_2 (5 wt.% Pd)	NaOAc	2	40
5	Pd_3P/SiO_2 (5 wt.% Pd)	KOH	2	70
6	Pd_3P/SiO_2 (5 wt.% Pd)	K_2CO_3	2	56
7	Pd_3P/SiO_2 (5 wt.% Pd)	Et_3N	1	80
8	Pd/SiO_2 (5 wt.% Pd)	Et_3N	1	50
9	Pd_3P/SiO_2 (1 wt.% Pd)	Et_3N	1	41

Reaction conditions: iodobenzene (1 mmol), base (3 mmol), CO (6 bar), ethanol (4 mL), catalyst (Pd 0.5 mol %), 100 °C, 1000 rpm.

To investigate the impact of the introduction of phosphorus, the synthesized palladium phosphide catalysts and the reference system, Pd/SiO_2 (5 wt.% Pd), were further investigated in the alkoxycarbonylation of iodobenzene. Clearly, Pd_3P/SiO_2 (5 wt.% Pd) exhibited a significantly higher activity than Pd/SiO_2 (5 wt.% Pd), demonstrating the impact of the d-metal-p-block element combination strategy (Table 1 and S1). A turn over frequency (TOF), calculated based on

dispersion measurement with CO chemisorption, of 7600 h^{-1} was determined for the alkoxycarbonylation of iodobenzene at 100 °C with Pd_3P/SiO_2 (5 wt.% Pd), whereas the application of Pd/SiO_2 (5 wt.% Pd) resulted in a substantially lower TOF of 2900 h^{-1} (Table S1). This is remarkable, since the CO dispersion measurements have initially shown a higher dispersion of the palladium-based reference catalyst. Similar results were observed at higher levels of conversions as depicted in Figure 3b. An iodobenzene conversion of 80 % (Table 1, entry 7) was observed after 1 h reaction time with Pd_3P/SiO_2 (5 wt.% Pd), while only 50 % conversion (Table 1, entry 8) could be achieved with the reference catalysts Pd/SiO_2 (5 wt.% Pd).

The significant enhancement in catalytic activity observed for Pd_3P/SiO_2 (5 wt.% Pd) compared to Pd/SiO_2 (5 wt.% Pd) strongly suggests that the improved performance stems from the unique crystal structure and surface arrangement of the palladium phosphide. Whereas uninterrupted Pd sites are observed in the crystal structure of pure palladium, the incorporation of phosphorus disrupts these contiguous sites, which results in the formation of separated active sites in palladium phosphide. An analysis of lower miller index surfaces of Pd_3P, reveals interatomic distances of neighboring Pd atoms ranging from 2.78 Å to 3.24 Å in Pd_3P (100), up to 2.93 Å in Pd_3P (001) until 3.11 Å in Pd_3P (010), all of which are longer in comparison to the uniform Pd–Pd distance of 2.75 Å in elemental Pd.[45] Furthermore, the surface structures indicate the formation of various isolated Pd ensembles, which may act as potential active sites (Figure S8). The site isolation in Pd_3P, combined with the increased Pd interatomic distances, suggests that the oxidative addition, which is the crucial first step in the catalytic cycle,[40] will be more favorable for bulkier aromatic halides on Pd_3P surfaces compared to pure Pd. This is attributed to a reduced steric hindrance, which significantly enhances catalytic activity. Additionally, the electronic effects induced by phosphorus[37] play a crucial role in optimizing the binding energy of substrates and intermediates

on the active sites. These combined factors, namely the tailored steric and electronic properties, contribute to the exceptional performance of the Pd_3P/SiO_2 (5 wt.% Pd) catalyst.

To further enhance the catalytic activity of Pd_3P, the effect of reducing its particle size was investigated by employing a lower Pd loading of 1 wt.%. Clear evidence of the crystallite size reduction was observed via PXRD measurements (Figure S2), where the absence of distinct reflections due to extreme line broadening confirmed the decreased particle size. Surprisingly, the use of Pd_3P/SiO_2 (1 wt.% Pd) as catalyst showed a negative impact on the catalytic activity, as a substantial reduction in conversion was observed in comparison to Pd_3P/SiO_2 (5 wt.% Pd). The alkoxycarbonylation of iodobenzene with ethanol yielded a conversion of only 41% (Table 1, entry 9) after 1 h at 100 °C and a CO pressure of 6 bar using Pd_3P/SiO_2 (1 wt.% Pd). In contrast, a significantly higher conversion of 80% was achieved under the same reaction conditions with Pd_3P/SiO_2 (5 wt.% Pd). The decline in activity when using lower palladium phosphide loadings may be attributed to surface poisoning effects, which are most likely caused by the strong binding of substrates or intermediates to the extremely small nanoparticles of the Pd_3P/SiO_2 catalyst (1 wt.% Pd).

The kinetics of heterogeneous alkoxycarbonylation reactions have been largely unexplored in many literature-reported systems. To address this gap, an investigation was conducted to determine the apparent activation energy of the Pd_3P/SiO_2 (5 wt.% Pd) catalyst to provide valuable insights into its catalytic behavior. The experiments were performed in the temperature range of 60-80 °C and the apparent activation energy for the alkoxycarbonylation of iodobenzene was estimated from the Arrhenius plot (ln (rate) v/s 1/T) to amount 98 ± 19 kJ/mol. The estimated apparent activation energy is comparable with the value reported by Ito *et al.* (104 kJ/mol) for the alkoxycarbonylation

of iodobenzene with palladium black,[42] whereby the underlying Arrhenius plot is based on rate constants and a higher temperature range (70-100 °C).

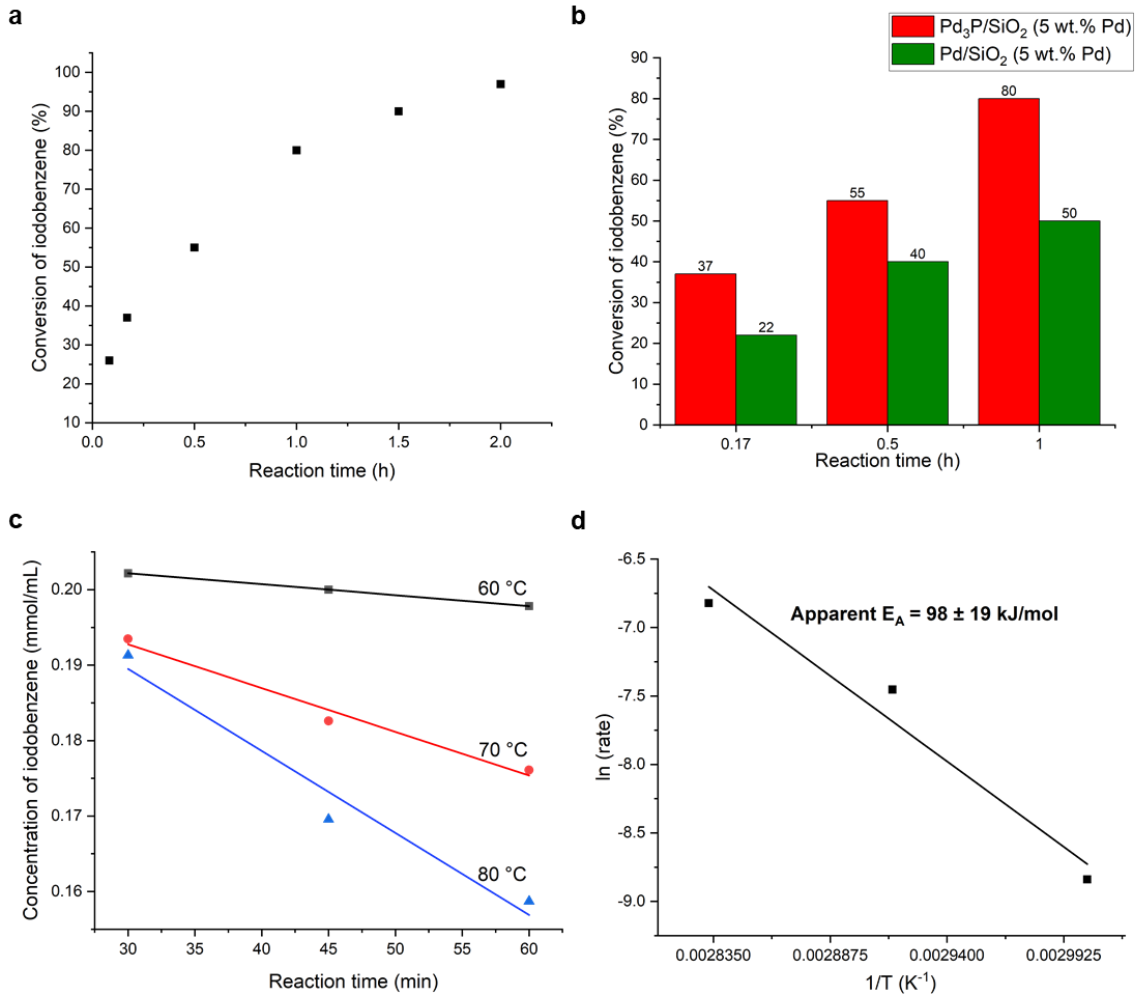

Figure 3: a) Conversion data for the alkoxycarbonylation of iodobenzene using Pd_3P/SiO_2 (5 wt.% Pd) and b) activity comparison with Pd/SiO_2 (5 wt.% Pd). Reaction conditions: iodobenzene (1 mmol), Et_3N (3 mmol), CO (6 bar), ethanol (4 mL), catalyst (Pd 0.5 mol %), 100 °C. c) Determination of the reaction rate at various temperatures and d) Arrhenius plot for the estimation of the apparent activation energy of the Pd_3P/SiO_2 (5 wt.% Pd) catalyst. Reaction conditions: iodobenzene (1 mmol), Et_3N (3 mmol) CO (6 bar), ethanol (4 mL), catalyst (Pd 0.5 mol %), 1000 rpm.

3.2.1. Substrate and reaction scope

After the successful application of Pd_3P/SiO_2 (5 wt.% Pd) in the alkoxycarbonylation of iodobenzene with ethanol, other alcohols such as methanol and isopropanol were explored as NuH and conversions of 97 and 96 % were observed, respectively (Table S2). Further, the substrate scope was extended towards substituted aryl halides, which resulted in excellent conversions ranging from 98 to 100 % for the ethoxycarbonylation of iodotoluene, bromo-iodobenzene and iodo-anisole (Table S2). Further, the applicability of the catalyst towards various carbonylation reactions were assessed considering amino and phenoxycarbonylation reactions. Aminocarbonylation reactions were performed in toluene as solvent with iodobenzene and aniline as substrates in the temperature range of 100 to 140 °C and 10 bar carbon monoxide pressure. An iodobenzene conversion of only 10 % to benzanilide was observed at 100 °C after 5 h reaction time, whereas a significantly enhanced conversion of 80 % was obtained with an increased temperature of 140 °C (Table S3). A preliminary test conducted for the phenoxycarbonylation of iodobenzene in toluene as solvent using Pd_3P/SiO_2 (5 wt.% Pd) as catalyst at 100 °C for 7 h resulted in 30 % conversion to phenyl benzoate (Table S2). All these results demonstrate the remarkable versatility of the synthesized Pd_3P/SiO_2 (5 wt.% Pd) catalyst, showcasing its exceptional ability to catalyze a broad spectrum of carbonylation reactions. Furthermore, the catalyst exhibits outstanding compatibility with a wide range of substituted aryl iodides and alcohols (NuH), which underscores its adaptability in diverse reaction conditions.

3.2.2. Recyclability studies

In order to assess the reusability of Pd_3P/SiO_2 (5 wt.% Pd), the catalyst was recovered after the reaction (first run) by centrifugation and again used for the aloxycarboylation of iodobenzene. No

decline in activity was observed in the first round of recycle giving 97 % conversion after 2h. However, a substantial reduction of conversion to 50 % was observed in the second round of recycling (Table S6). The palladium content in the recovered catalyst from the first run was quantified via ICP-AES analysis to estimate the precious metal loss during the process. A reduction of palladium loading from 4.94 to 3.70 wt.% was determined, which indicates a severe loss of Pd_3P nanoparticles due to applied reaction conditions and mechanical milling induced by the fast-rotating stirrer in the batch autoclave. The transmission electron microscopy analysis of the recovered Pd_3P/SiO_2 (5 wt.% Pd) catalysts showed an increase in the particle size from 5.56 nm to 7.01 nm after the first run, revealing the sintering of nanoparticles under the applied reaction conditions (Figure S4). Such aggregation of palladium nanoparticles, facilitated by carbon monoxide is a well-known phenomenon,[1,18] and can therefore be considered as the reason for the increased particle size in the recovered catalyst, which ultimately leads to a subsequent decline in catalytic activity. However, the structural integrity of the recovered catalyst was confirmed through HRTEM lattice fringe-based assessment, were the d spacing of 2.0 Å corresponding to Pd_3P (122) indicates (Figure S5) no phase transition or decomposition during catalysis. The loss of nanoparticles from the support also became obvious from the Tindall effect observed in the supernatant. These findings indicate the necessity of further investigations to improve the support-nanoparticle interaction to avoid leaching of the metal phosphide from the support. In this context, other support materials, such as phosphorus modified silica, which led to a substantial reduction in Pd leaching in Heck coupling reaction,[38] modified carbon or ceria, or metal organic frameworks as supports, can be investigated to suppress the loss of palladium phosphide nanoparticles.

3.3 Heterogeneously versus homogeneously catalyzed alkoxycarbonylation reactions

Further, the activities of homogeneous catalysts, such as palladium acetate ($Pd(OAc)_2$) and palladium nitrate ($Pd(NO_3)_2 \cdot 2H_2O$), were explored in the alkoxycarbonylation of iodobenzene and turn over frequencies were estimated for comparison reasons. The TOF values of $Pd(OAc)_2$ (618 h^{-1}) and $Pd(NO_3)_3 \cdot 2H_2O$ (698 h^{-1}) were found to be significantly lower compared to those of Pd_3P/SiO_2 (5 wt.% Pd), which exhibited a TOF of 7600 h^{-1} under identical reaction conditions (Table S4). These findings again underline the superior catalytic performance of the synthesized palladium phosphide catalyst. To evaluate the performance of the synthesized catalysts relative to other reported systems further, a comparison with other heterogenous catalysts was conducted based on the conversion of iodobenzene under similar reaction conditions (Table S5). The data reveal that Pd_3P/SiO_2 (5 wt.% Pd) outperforms many reported heterogeneous catalysts, demonstrating the effectiveness of the d-block–p-block element combination strategy in the alkoxycarbonylation of aryl iodides.

4. Conclusions

The application of element synergy, which involves the incorporation of a non-metal from the p-block into a metal matrix, represents a highly effective strategy for designing high-performance heterogeneous catalysts. This approach has now been further extended to the field of carbonylation reactions, including alkoxycarbonylation, aminocarbonylation and phenoxycarbonylation reactions. In this study, the incorporation of phosphorus into palladium resulted in the formation of highly active supported Pd_3P nanoparticles, which demonstrated superior performance compared to conventionally supported Pd nanoparticles and even outperformed several homogeneous catalysts. The exceptional catalytic activity of Pd_3P/SiO_2 can be attributed to two

key factors: the formation of well-defined, isolated active palladium sites on the catalyst surface and the electronic modulation induced by phosphorus. Similar to the role of a ligand in molecular complexes, phosphorus modifies the electronic and geometric properties of the metal, which significantly enhanced the catalytic performance. This work underscores the immense potential of element synergy in the rational design of heterogeneous catalysts, paving the way for new advancements in carbonylation chemistry.

Acknowledgements

The authors gratefully acknowledge the funding for A.N. from BASF and the productive discussions with the team at hte GmbH. The authors would like to thank Ms. Kathrin Schaefer (ITCP, KIT) for performing CO chemisorption measurements. This study was also supported by the Deutsche Forschungsgemeinschaft (DFG, German Research Foundation) -SFB 1441- Project-ID 426888090. We also would like to express our gratitude to the NFDI4Cat community, which is funded by the Deutsche Forschungsgemeinschaft (DFG, German Research Foundation) - Project-ID 441926934, for valuable discussions.

Conflict of interest

The authors of this article (A.N., S.H, S.A.S) have applied for a patent relating to the content of this articles.

References

[1] B. Urbán, M. Papp, R. Skoda-Földes, *Curr. Green Chem.* **2019**, *6*, 78–95.

[2] J. M. Tukacs, B. Marton, E. Albert, I. Tóth, L. T. Mika, *J. Organomet. Chem.* **2020**, *923*, 121407.

[3] A. Brennführer, H. Neumann, M. Beller, *Angew. Chem. Int. Ed.* **2009**, *48*, 4114–4133.

[4] M. V. Khedkar, T. Sasaki, B. M. Bhanage, *ACS Catal.* **2013**, *3*, 287–293.

[5] F. Messa, A. N. Paparella, D. Veselý, J. Krajčovič, P. Papadia, S. Perrone, A. Salomone, *European J. Org. Chem.* **2023**, *26*, e202300309.

[6] C. F. J. Barnard, *Org. Process Res. Dev.* **2008**, *12*, 566–574.

[7] A. Schoenberg, I. Bartoletti, R. F. Heck, *J. Org. Chem.* **1974**, *39*, 3318–3326.

[8] W. Mägerlein, M. Beller, A. F. Indolese, *J. Mol. Catal. A Chem.* **2000**, *156*, 213–221.

[9] A. Yamamoto, F. Ozawa, N. Kawasaki, H. Okamoto, T. Yamamoto, *Organometallics* **1987**, *6*, 1640–1651.

[10] B. Apanda, S. Zolezzi, G. Valdebenito, J. Cáceres-vásquez, S. A. Moya, P. Aguirre, *J. Chil. Chem. Soc.* **2013**, *58*, 2136–2137.

[11] E. Mizushima, T. Hayashi, M. Tanaka, *Green Chem.* **2001**, *3*, 76–79.

[12] H. Neumann, A. Brennführer, P. Groß, T. Riermeier, J. Almena, M. Beller, *Adv. Synth. Catal.* **2006**, *348*, 1255–1261.

[13] J. R. Martinelli, T. P. Clark, D. A. Watson, R. H. Munday, S. L. Buchwald, *Angew. Chem. Int. Ed.* **2007**, *46*, 8460–8463.

[14] T. Xu, H. Alper, *J. Am. Chem. Soc.* **2014**, *136*, 16970–16973.

[15] A. Mata, C. A. Hone, B. Gutmann, L. Moens, C. O. Kappe, *ChemCatChem* **2019**, *11*, 997–1001.

[16] J. R. Martinelli, D. A. Watson, D. M. M. Freckmann, T. E. Barder, S. L. Buchwald, *J. Org. Chem.* **2008**, *73*, 7102–7107.

[17] C. F. J. Barnard, *Organometallics* **2008**, *27*, 5402–5422.

[18] V. Dufaud, J. Thivolle-Cazat, J.-M. Basset, *J. Chem. Soc. Chem. Commun.* **1990**, 426.

[19] J. Liu, J. Chen, C. Xia, *J. Catal.* **2008**, *253*, 50–56.

[20] F. Chen, T. Li, X. Pan, Y. Guo, B. Han, F. Liu, B. Qiao, A. Wang, T. Zhang, *Sci. China Mater.* **2020**, *63*, 959–964.

[21] A. Siva Prasad, B. Satyanarayana, *J. Mol. Catal. A Chem.* **2013**, *370*, 205–209.

[22] I. Ziccarelli, H. Neumann, C. Kreyenschulte, B. Gabriele, M. Beller, *Chem. Commun.* **2016**, *52*, 12729–12732.

[23] Y. Zhang, Y. Xiong, J. Ge, R. Lin, C. Chen, Q. Peng, D. Wang, Y. Li, *Chem. Commun.* **2018**, *54*, 2796–2799.

[24] H. Mei, S. Xiao, T. Zhu, Y. Lei, G. Li, *Transit. Met. Chem.* **2014**, *39*, 443–450.

[25] M. B. Ibrahim, R. Suleiman, M. Fettouhi, B. El Ali, *RSC Adv.* **2016**, *6*, 78826–78837.

[26] V. V. Gaikwad, V. B. Saptal, K. Harada, T. Sasaki, D. Nishio-Hamane, B. M. Bhanage, *ChemNanoMat* **2018**, *4*, 575–582.

[27] B. Liu, X. Lan, Q. Zhong, T. Wang, *ACS Catal.* **2024**, 757–775.

[28] S. Hanf, L. Alvarado Rupflin, R. Gläser, S. Schunk, *Catalysts* **2020**, *10*, 510.

[29] D. Albani, M. Shahrokhi, Z. Chen, S. Mitchell, R. Hauert, N. López, J. Pérez-Ramírez, *Nat.*

Commun. **2018**, *9*, 1–11.

[30] A. Neyyathala, E. Fako, S. De, D. Gashnikova, F. Maurer, J. Grunwaldt, S. A. Schunk, S. Hanf, *Small Struct.* **2025**, *6*, 2400260.

[31] L. Alvarado Rupflin, J. Mormul, M. Lejkowski, S. Titlbach, R. Papp, R. Gläser, M. Dimitrakopoulou, X. Huang, A. Trunschke, M. G. Willinger, R. Schlögl, F. Rosowski, S. A. Schunk, *ACS Catal.* **2017**, *7*, 3584–3590.

[32] A. Neyyathala, F. Flecken, S. Hanf, *Chempluschem* **2023**, *88*, e202200431.

[33] S. Vásquez-Céspedes, R. C. Betori, M. A. Cismesia, J. K. Kirsch, Q. Yang, *Org. Process Res. Dev.* **2021**, *25*, 740–753.

[34] J. Masud, T. Van Nguyen, N. Singh, E. McFarland, M. Ikenberry, K. Hohn, C.-J. Pan, B.-J. Hwang, *J. Electrochem. Soc.* **2015**, *162*, F455–F462.

[35] D. Albani, K. Karajovic, B. Tata, Q. Li, S. Mitchell, N. López, J. Pérez-Ramírez, *ChemCatChem* **2019**, *11*, 457–464.

[36] E. Nishiwaki, P. S. Rice, D.-Y. Kuo, F. Y. Dou, A. Pyka, B. Reid, H. A. Nguyen, E. M. Stuve, S. Raugei, B. M. Cossairt, *Chem. Commun.* **2024**, *60*, 6941–6944.

[37] B. Liu, N. Huang, Y. Wang, X. Lan, T. Wang, *ACS Catal.* **2021**, *11*, 1787–1796.

[38] A. Neyyathala, F. Flecken, F. Rang, C. Papke, S. Hanf, *Chem. Eur. J.* **2024**, *30*, e202302825.

[39] S. Carenco, Y. Hu, I. Florea, O. Ersen, C. Boissière, N. Mézailles, C. Sanchez, *Chem. Mater.* **2012**, *24*, 4134–4145.

[40] P. E. Garrou, R. F. Heck, *J. Am. Chem. Soc.* **1975**, *4115*, 4115–4127.

[41] Y. Hu, J. Liu, Z. Lu, X. Luo, H. Zhang, Y. Lan, A. Lei, *J. Am. Chem. Soc.* **2010**, *132*, 3153–3158.

[42] T. Ito, K. Mori, T. Mizoroki, A. Ozaki, *Bull. Chem. Soc. Jpn.* **1975**, *48*, 2091–2094.

[43] R. S. Mane, T. Sasaki, B. M. Bhanage, *RSC Adv.* **2015**, *5*, 94776–94785.

[44] S. M. Islam, K. Ghosh, A. S. Roy, R. A. Molla, *RSC Adv.* **2014**, *4*, 38986–38999.

[45] Y. Liu, A. J. McCue, C. Miao, J. Feng, D. Li, J. A. Anderson, *J. Catal.* **2018**, *364*, 406–414.